Epitaxial Bi₂Sr₂CuOᵧ thin films as p-type transparent conductors

Chen Zhou(周臣), Wang-Ping Cheng(程王平), Yuan-Di He(何媛娣), Cheng Shao(邵成), Ling Hu(胡令), Ren-Huai Wei(魏仁怀), Jing-gang Qin(秦经刚), Wen-Hai Song(宋文海), Xue-Bin Zhu(朱雪斌), Chuan-Bing Cai(蔡传兵), and Yu-Ping Sun(孙玉平)

What follows is a list of articles you may be interested in

Laser-induced phase conversion of n-type SnSe₂ to p-type SnSe

Qi Zheng(郑琦), Rong Yang(杨蓉), Kang Wu(吴康), Xiao Lin(林晓), Shixuan Du(杜世萱), Chengmin Shen(申承民), Lihong Bao(鲍丽宏), and Hong-Jun Gao(高鸿钧)
Chin. Phys. B, 2022, 31 (**4**): 047306.   DOI: 10.1088/1674-1056/ac4901

Investigation on threshold voltage of p-channel GaN MOSFETs based on p-GaN/AlGaN/GaN heterostructure

Ruo-Han Li(李若晗), Wu-Xiong Fei(费武雄), Rui Tang(唐锐), Zhao-Xi Wu(吴照玺), Chao Duan(段超), Tao Zhang(张涛), Dan Zhu(朱丹), Wei-Hang Zhang(张苇杭), Sheng-Lei Zhao(赵胜雷), Jin-Cheng Zhang(张进成), and Yue Hao(郝跃)
Chin. Phys. B, 2021, 30 (**8**): 087305.   DOI: 10.1088/1674-1056/ac0793

Novel fast-switching LIGBT with P-buried layer and partial SOI

Haoran Wang(王浩然), Baoxing Duan(段宝兴), Licheng Sun(孙李诚), and Yintang Yang(杨银堂)
Chin. Phys. B, 2021, 30 (**2**): 027302.   DOI: 10.1088/1674-1056/abcf3e

Band alignment of p-type oxide/ε-Ga₂O₃ heterojunctions investigated by x-ray photoelectron spectroscopy

Chang Rao(饶畅), Zeyuan Fei(费泽元), Weiqu Chen(陈伟驱), Zimin Chen(陈梓敏), Xing Lu(卢星), Gang Wang(王钢), Xinzhong Wang(王新中), Jun Liang(梁军), Yanli Pei(裴艳丽)
Chin. Phys. B, 2020, 29 (**9**): 097303.   DOI: 10.1088/1674-1056/ab9c0d

Multi-carrier transport in ZrTe₅ film

Fangdong Tang(汤方栋), Peipei Wang(王培培), Peng Wang(王鹏), Yuan Gan(甘远), Le Wang(王乐), Wei Zhang(张威), Liyuan Zhang(张立源)
Chin. Phys. B, 2018, 27 (**8**): 087307.   DOI: 10.1088/1674-1056/27/8/087307

Epitaxial Bi$_2$Sr$_2$CuO$_y$ thin films as p-type transparent conductors

Chen Zhou(周臣)[1,2], Wang-Ping Cheng(程王平)[1,2], Yuan-Di He(何媛娣)[1,2], Cheng Shao(邵成)[1],
Ling Hu(胡令)[1], Ren-Huai Wei(魏仁怀)[1,†], Jing-Gang Qin(秦经刚)[3,‡], Wen-Hai Song(宋文海)[1],
Xue-Bin Zhu(朱雪斌)[1,§], Chuan-Bing Cai(蔡传兵)[4], and Yu-Ping Sun(孙玉平)[1,5,6]

[1] *Key Laboratory of Materials Physics, Institute of Solid State Physics, HFIPS, Chinese Academy of Sciences, Hefei 230031, China*
[2] *University of Science and Technology of China, Hefei 230026, China*
[3] *Institute of Plasma Physics, Chinese Academy of Sciences, HFIPS, Chinese Academy of Sciences, Hefei 230031, China*
[4] *Physics Department, Shanghai Key Laboratory of High Temperature Superconductors, Shanghai University, Shanghai 200444, China*
[5] *High Magnetic Field Laboratory, HFIPS, Chinese Academy of Sciences, Hefei 230031, China*
[6] *Collaborative Innovation Centre of Advanced Microstructures, Nanjing University, Nanjing 210093, China*

Development of p-type transparent conducting thin films is tireless due to the trade-off issue between optical transparency and conductivity. The rarely concerned low normal state resistance makes Bi-based superconducting cuprates the potential hole-type transparent conductors, which have been realized in Bi$_2$Sr$_2$CaCu$_2$O$_y$ thin films. In this study, epitaxial superconducting Bi$_2$Sr$_2$CuO$_y$ and Bi$_2$Sr$_{1.8}$Nd$_{0.2}$CuO$_y$ thin films with superior normal state conductivity are proposed as p-type transparent conductors. It is found that the Bi$_2$Sr$_{1.8}$Nd$_{0.2}$CuO$_y$ thin film with thickness 15 nm shows an average visible transmittance of 65% and room-temperature sheet resistance of 650 Ω/sq. The results further demonstrate that Bi-based cuprate superconductors can be regarded as potential p-type transparent conductors for future optoelectronic applications.

1. Introduction

It is well known that p-type transparent conductors (TCs) with positive charges carrying an electrical current are the most crucial components in future invisible active circuit devices.[1–4] However, research on p-type TCs is still in their infancy. Many materials fail to combine acceptable electrical conductivity and optical transparency, which renders them unable to compete with n-type TCs. The difficulty of converting oxides from n-type to p-type via acceptor-doping is due to the localized O 2p-derived valence band, which impedes the introduction of shallow acceptors and large hole-type effective mass.[5] The strategy of "chemical modulation of the valence band" promotes the development of p-type TCs, and the Cu-based delafossite oxide CuMO$_2$ (M = Al, Cr, Ga, Y, etc.) are extensively investigated in recent years.[6–12] However, carrier compensation and structural deformations hamper the improvement of the optoelectronic performance of these oxides, especially for the conductivity at room temperature.[13]

Starting from a conductor that already has plenty of free carriers may be possible if the bulk metals have a sufficiently wide energy window in their electronic structure above Fermi energy E_F and a low screened plasma energy $\hbar\omega_p$, to ensure optical transparency.[14] The screened plasma energy $\hbar\omega_p$ can be described by $\hbar\omega_p = \hbar(e^2/\varepsilon_0\varepsilon_r)^{1/2}(n/m^*)^{1/2}$, where $\hbar$ is the reduced Planck constant, ε_0 is the vacuum permittivity, ε_r is the relative permittivity, n is the carrier concentration, and m^*

is the carrier effective mass.[15] On the other hand, the conductivity of a material is up to $\sigma = nq\mu = q^2\tau(n/m^*)$, in which q is the elemental charge, μ is the carrier mobility, and τ is the scattering time. The two contradictory properties including conductivity and transmittance can be simultaneously improved by selecting appropriate materials with both high n and m^*, namely, correlated metals.[15] The new effective strategy for the design of TC thin films has been achieved in n-type alkaline earth-based vanadates, molybdates and niobates.[15–21]

Bi-based cuprates, Bi$_2$Sr$_2$Ca$_{n-1}$Cu$_n$O$_y$ (n = 1, 2, 3), simultaneously possess heavy hole carriers and high carrier concentrations, which can shift the screened plasma energy to the near-infrared region below 1.75 eV and will not obscure optical transparency.[22–26] For instance, the Bi$_2$Sr$_2$CaCu$_2$O$_y$ (Bi-2212) with $\hbar\omega_p$ = 1.6 eV has been proved to be p-type TC with excellent optoelectronic performance.[27]

The compound Bi$_2$Sr$_2$CuO$_y$ (Bi-2201), which has a similar layered crystal structure to Bi-2212, can potentially be utilized as effective p-type TCs due to the following reasons. Firstly, the Bi-2201 has a lower room temperature resistivity than that of Bi-2212 and Bi$_2$Sr$_2$Ca$_2$Cu$_3$O$_y$ (Bi-2223).[28–32] Secondly, the Bi-2201 single crystal with a lower carrier mean free path of 1.9 nm can be reduced to several nanometers without obvious depress of the electrical transport properties.[23] Moreover, the screened plasma energy $\hbar\omega_p$ is 1.0 eV, indicating that the itinerant electrons may react slowly

with the incoming light wave and further avoid screening and reflection.[23]

In this study, the epitaxial superconducting Bi-2201 and $Bi_2Sr_{1.8}Nd_{0.2}CuO_y$ ((Bi,Nd)-2201) thin films were synthesized by a solution method. It is found that the p-type Bi-2201 and (Bi,Nd)-2201 thin films with lower thickness display excellent performance of optical transmittance in the visible-to-near-infrared range, while possessing low room-temperature sheet resistance.
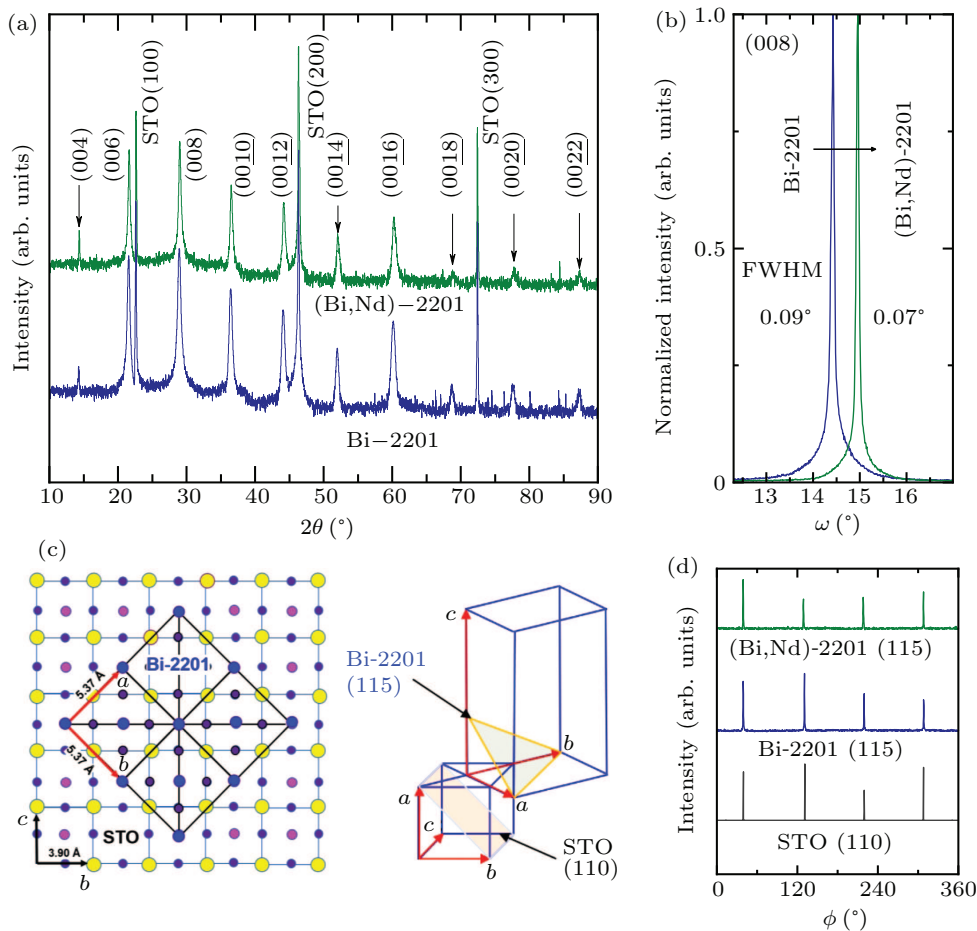
2. Experimental details

First, the precursor solutions were prepared by dissolving stoichiometric bismuth acetate ($Bi(CH_3COO)_3$, 5% over-weighted to compensate for the volatilization of Bi), strontium acetate ($Sr(CH_3COO)_2 \cdot 0.5H_2O$), copper acetate ($Cu(CH_3COO)_2 \cdot H_2O$) and neodymium acetate ($Nd(CH_3COO)_3 \cdot xH_2O$)) into propionic acid. Before the deposition procedure, the single crystal of $SrTiO_3$ (STO) (100) substrates was ultrasonically cleaned in acetone, ethanol, and deionized water in steps, followed by a final cleaning process using a plasma cleaner under argon. Spin-coating technology was used to coat the former solutions. The as-deposited wet thin films were baked at 120 °C for 1 min and pyrolyzed at 350 °C for 10 min to eliminate residual organics. The obtained amorphous coatings were calcined at 780 °C for 30 min in air. The above procedures were cycled several times to tune the final film thickness.

High-resolution x-ray diffraction (XRD, Philips X'Pert Pro) with $\theta/2\theta$ scans was performed to check the thin film phases and orientations. The rocking curves for the Bi-based cuprate thin films were checked by $2\theta/\omega$ scans. X-ray phi-scans were also carried out for all Bi-2201 and (Bi,Nd)-2201 thin films to check the epitaxial relationships between thin films and substrates. An atomic force microscope (NX10, Park Systems Crop., Korea) was used to determine the thin film thickness and surface morphology, respectively. Resistivity and the Hall coefficient were measured by using the standard four-gold-probe method and the van der Pauw geometry, respectively, on a Quantum Design physical property measurement system (PPMS-9T). Room-temperature transmission spectra for all thin films were obtained using the UV/Vis/NIR spectrometer (VARIAN, CARY-5E).

3. Results and discussion

The detailed structural characteristics of the Bi-2201 and (Bi,Nd)-2201 thin films are presented in Fig. 1.

Fig. 1. (a) Out-of-plane XRD profiles for the Bi-2201 and (Bi,Nd)-2201 thin films grown on STO (100) substrates. (b) Rocking curves of (008) peaks for the above two thin films. (c) Schematic diagram of the epitaxial relationship between the thin film and the substrate. (d) XRD ϕ-scans of reflections for the STO (110), Bi-2201 and (Bi,Nd)-2201 (115) crystal plane.

As can be seen from the out-of-plane XRD profiles in Fig. 1(a), only (00l)-orientated diffraction peaks can be detected for both thin films, indicating that phase-pure Bi-based cuprate can be derived by a simple solution deposition method. The c-axis lattice constant is determined to be 25.52 Å for Bi-2201 and 25.42 Å for (Bi,Nd)-2201 based on the Bragg formula, $2d\sin\theta = n\lambda$. The decreasing lattice constant can also be detected by the shift of rocking curve for the Bi-2201 and 10%Nd-doped one, as displayed in Fig. 1(b). In addition, both thin films show narrow full width of half maximum (FWHM) below 0.1°. For the Bi-2201 thin films grown on the STO substrates, the optimum matched mode can be sketched in Fig. 1(c) from the point of the geometrical relationship. The a-axis lattice constant of the cubic STO is 3.91 Å, while the tetragonal Bi-2201 is 5.37 Å, indicating that the unit cell of Bi-2201 should rotate 45° to fulfill the epitaxial relationship between the film and substrate. Therefore, the plane (110) of the STO is parallel to the plane (115) of Bi-2201, as also seen in the right portion of Fig. 1(c). The above two thin films were checked by azimuthal scans to verify this growth mechanism. Figure 1(d) shows that the fourfold symmetry of the (115)-plane for the Bi-2201 is corresponding to the (110)-plane of the STO, confirming the epitaxial relationship of (115)film∥(110)substrate.

Figure 2 displays the surface morphology of the Bi-2201 and (Bi,Nd)-2201 thin films to check the surface characteristic and roughness when downsizing the film thickness. All thin films show homogeneous and smooth surfaces. Bi-2201 films show that the root-mean-square (rms) roughness decreases from 5.135 nm to 1.639 nm with decreasing film thickness. It is interesting to observe that the Nd-doped Bi-2201 thin films display lower rms roughness (4.209 nm to 0.476 nm) than that of the matrix film with the same thickness. The optimized smooth surface obtained by doping Nd in Bi-2201 can effectively decrease the surface carrier scattering, especially for thin films with lower thickness.

Figure 3(a) gives the resistivity ρ versus temperature behavior for the Bi-2201 and (Bi,Nd)-2201 thin films with different thicknesses. It is shown that thin films with thickness of 45 nm and 80 nm present superconducting transition at low temperatures. However, the superconducting behavior vanishes when the thickness downsizes to 30 nm for both the Bi-2201 and (Bi,Nd)-2201 thin films. At room temperature (300 K), the resistivity shows a predictable increasing trend with decreasing film thickness. As seen in Fig. 3(c), however, the rising extent of room temperature resistivity is much lower for the (Bi,Nd)-2201 thin films than that of the Bi-2201, which can largely be due to the evolution of surface morphol-

ogy, as presented in Fig. 2. Based on the results of the carrier concentration determined by Hall measurements in Fig. 3(d), Nd-doping in Bi-2201 declines the hole-like carriers. The decreasing carrier concentration (n_h) for (Bi,Nd)-2201 can be elucidated by electron doping in Sr sites, as also commonly observed in La-doped Bi-2201.[33] Moreover, it is seen from Fig. 3(e) that the carrier mobility (μ_h) increases with increasing film thickness. The (Bi,Nd)-2201 thin films display larger room temperature mobility than that of the host film, which is mainly due to the enhancement of film quality based on the lower rocking curve FWHM (Fig. 1(b)) and optimized smooth surface (Fig. 2). It should be noted here that the hole mobility with the value of 1.4–2.1 cm^2/V·s for the (Bi,Nd)-2201 thin film is much larger than that of recent reported p-type TC films.[26,34,35] Figure 3(f) gives the room temperature Hall resistance (R_{xy}) versus measured magnetic field (B) for the 80-nm-thick films, and the positive Hall coefficients confirm that both the Bi-2201 and (Bi,Nd)-2201 thin films are hole-type.
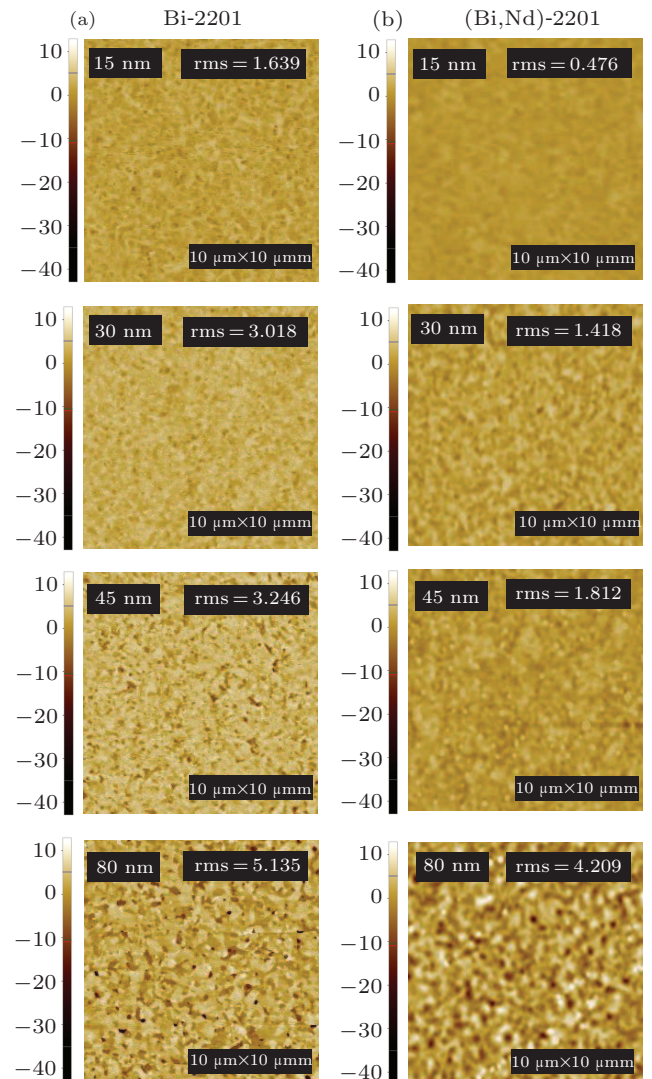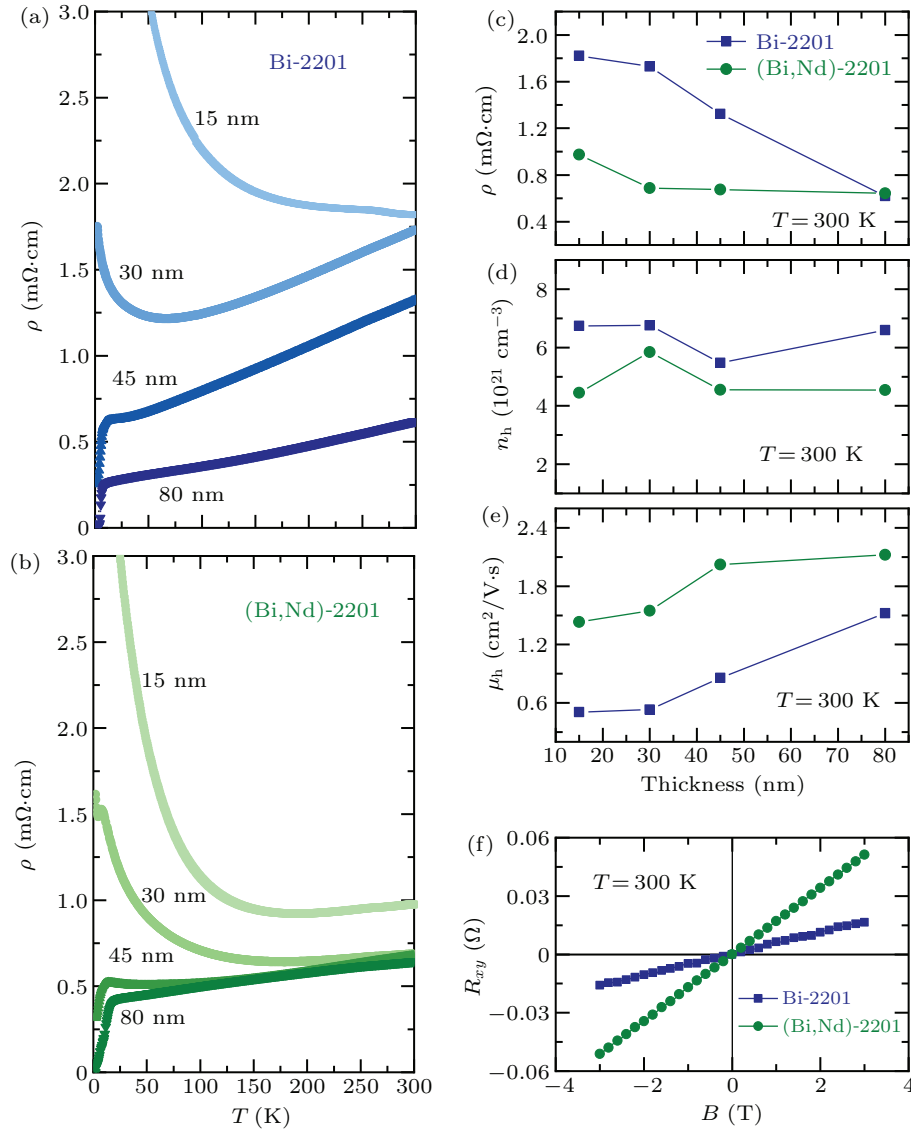

Fig. 2. Surface morphologies of (a) Bi-2201 and (b) (Bi,Nd)-2201 thin films with different thicknesses.
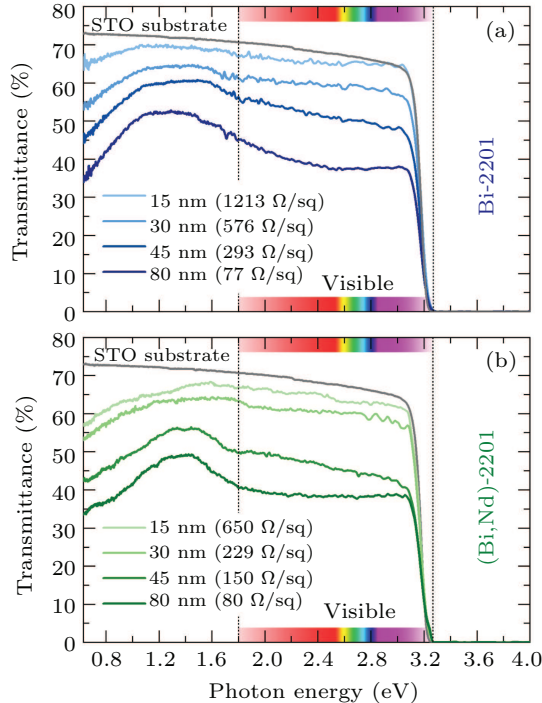
Fig. 3. Temperature dependent resistivity in the range of 300–2 K for the different-thickness (a) Bi-2201 thin films and (b) (Bi,Nd)-2201 thin films. Plots of (c) resistivity, (d) hole density and (e) hole mobility of Bi-2201 and (Bi, Nd)-2201 thin films versus film thickness at room temperature. (f) Evolution of room-temperature Hall resistance with magnetic field for the above two thin films.
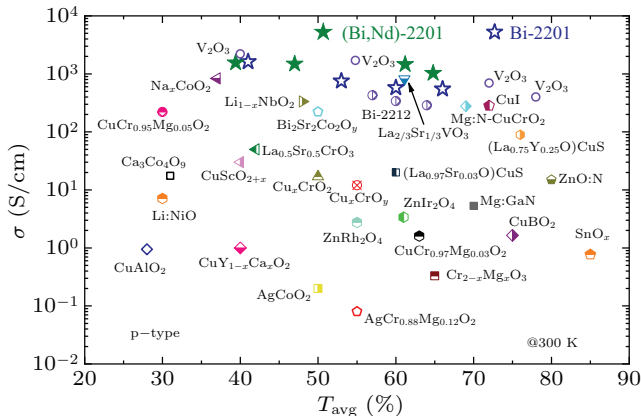
Figure 4 shows the optical transmittance (T_{opt}) of the different-thickness Bi-2201 and (Bi,Nd)-2201 thin films. At near-infrared wavelength, all thin films show the decreasing trend with the decreasing of photon energy, which is mainly due to the carrier reflection. In the most important visible range, it can be clearly seen that the transmittance increases over 20% for both thin films when the film thickness decreases from 80 nm to 15 nm. Such an optimized route through dimensionality reduction is an effective approach to developing neoteric TC materials in either n-type or p-type.[15,16,18,19,27,34,35] The 15-nm-thick Bi-2201 and (Bi,Nd)-2201 thin films show excellent average transmittance of 66% and 65%, while maintaining low room-temperature resistivity of 1.82 mΩ·cm and 0.97 mΩ·cm (Fig. 3(c)) and sheet resistance of 1213 Ω/sq and 650 Ω/sq, respectively. As for the ultraviolet region, the sharp decrease of transmittance is due to intra-band absorption from the STO substrate.[36]

Figure 5 gives the graphical representation of room-temperature conductivity (σ) and visible average transmittance (T_{avg}) for the Bi-2201, (Bi,Nd)-2201 epitaxial films and other representative p-type transparent conducting thin films. It shows that Bi-2201 and (Bi,Nd)-2201 show larger room-temperature conductivity and higher optical transmittance than that of the Bi-2212 thin films and the overwhelming majority of p-type TCs. Our group has reported that the transparent conducting Bi-2212 films with the highest conductivity of 1064 S/cm (180 nm) and the highest transmittance of 65% (15 nm). However, when the film thickness is reduced to 15 nm, the conductivity of Bi-2212 drops to 288 S/cm.[27] Herein, the 80 nm Bi-2201 and (Bi,Nd)-2201 have 1615 S/cm and 1553 S/cm, respectively. The 15-nm-thick Bi-2201 and (Bi,Nd)-2201 thin films have a transmittance of 66% and 65% while maintaining the conductivity of 549 S/cm and 1025 S/cm, respectively. Moreover, all detailed parameters

corresponding Fig. 5 are listed in Table S1 in the supplementary material. It is seen that the p-type Bi-2201 and (Bi,Nd)-2201 TCs locate at the competitive values amongst reported p-type TCs so far, suggesting that the Bi-based cuprates are the promising candidate in p-type TC applications.

Fig. 4. Optical transmittance spectra for the bare STO (100), (a) Bi-2201 and (b) (Bi,Nd)-2201 thin films with different thicknesses. The corresponding room-temperature sheet resistance are given in the brackets.

Fig. 5. Summary of room-temperature conductivity σ and visible average transmittance T_{avg} for the Bi-2201, (Bi,Nd)-2201 and other representative p-type transparent conducting thin films.

4. Conclusion

In conclusion, epitaxial superconducting Bi2201 and (Bi,Nd)-2201 thin films have been fabricated and proposed as p-type transparent conductors. Nd doping in Bi2201 can effectively improve the film orientation and surface morphology. In addition, the average visible transmittance can be optimized to 65% through a dimensionality reduction, while maintaining a low room-temperature sheet resistance of 650 Ω/sq. Our study demonstrates that Bi-based cuprate superconductors can be fabricated by a simple solution route and are regarded as efficient p-type transparent conductors with excellent performance.

Supplementary material

See the supplementary material Table S1 for all detail parameters corresponding to Fig. 5.

References

[1] Wang Z, Nayak P K, Caraveo-Frescas J A and Alshareef H N 2016 *Adv. Mater.* **28** 3831
[2] Beyer W, Hupkes J and Stiebig H 2007 *Thin Solid Films* **516** 147
[3] Ohta H and Hosono H 2004 *Mater. Today* **7** 42
[4] Banerjee A and Chattopadhyay K 2005 *Prog. Cryst. Growth Charact. Mater.* **50** 52
[5] Kawazoe H, Yanagi H, Ueda K and Hosono H 2000 *MRS Bull.* **25** 28
[6] Kawazoe H, Yasukawa M, Hyodo H, Kurita M, Yanagi H and Hosono H 1997 *Nature* **389** 939
[7] Nagarajan R, Draeseke A D, Sleight A W and Tate J 2001 *J. Appl. Phys.* **89** 8022
[8] Jayaraj M K, Draeseke A D, Tate J and Sleight A W 2001 *Thin Solid Films* **397** 244
[9] Ueda K, Hase T, Yanagi H, Kawazoe H, Hosono H, Ohta H, Orita M and Hirano M 2001 *J. Appl. Phys.* **89** 1790
[10] Duan N and Sleight A W 2000 *Appl. Phys. Lett.* **77** 1325
[11] Snure M and Tiwari A 2007 *Appl. Phys. Lett.* **91** 092123
[12] Yanagi H, Hase T, Ibuki S, Ueda K and Hosono H 2001 *Appl. Phys. Lett.* **78** 1583
[13] Freeman A J, Poeppelmeier K R, Mason T O, Chang R P H and Marks T J 2000 *MRS Bull.* **25** 45
[14] Zhang X, Zhang L, Perkins J D and Zunger A 2015 *Phys. Rev. Lett.* **115** 176602
[15] Zhang L, Zhou Y, Guo L, Zhao W, Barnes A, Zhang H T, Eaton C, Zheng Y, Brahlek M, Haneef H F, Podraza N J, Chan M H W, Gopalan V, Rabe K M and Engel-Herbert R 2016 *Nat. Mater.* **15** 204
[16] Ha Y and Lee S 2020 *Adv. Funct. Mater.* **30** 2001489
[17] Stoner J L, Murgatroyd P A E, O'Sullivan M, Dyer M S, Man-ning T D, Claridge J B, Rosseinsky M J and Alaria J 2019 *Adv. Funct. Mater.* **29** 1808609
[18] Wells M P, Zou B, Doiron B G, Kilmurray R, Mihai A P, Oulton R F M, Gubeljak P, Ormandy K L, Mallia G, Harrison N M, Cohen L F, Maier S A, Alford N M N and Petrov P K 2017 *Adv. Opt. Mater.* **5** 1700622
[19] Park Y, Roth J, Oka D, Hirose Y, Hasegawa T, Paul A, Pogreb-nyakov A, Gopalan V, Birol T and Engel-Herbert R 2020 *Commun. Phys.* **3** 102
[20] Asmara T C, Wan D, Zhao Y, Majidi M A, Nelson C T, Scott M C, Cai Y, Yan B, Schmidt D, Yang M, Zhu T, Trevisanutto P E, Motapothula M R, Feng Y P, Breese M B H, Sherburne M, Asta M, Minor A, Venkatesan T and Rusydi A 2017 *Nat. Commun.* **8** 15271
[21] Wan D Y, Zhao Y L, Cai Y, Asmara T C, Huang Z, Chen J Q, Hong J, Yin S M, Nelson C T, Motapothula M R, Yan B X, Xiang D, Chi X, Zheng H, Chen W, Xu R, Ariando A R, Minor A M, Breese M B H, Sherburne M, Asta M, Xu Q H and Venkatesan T 2017 *Nat. Commun.* **8** 15070
[22] Uemura Y J, Luke G M, Sternlieb B J, Brewer J H, Carolan J F, Hardy W N, Kadono R, Kempton J R, Kiefl R F, Kreitzman S R, Mulhern P, Riseman T M, LL Williams D, Yang B X, Uchida S, Takagi H, Gopalakrishnan J, Sleight A W, Subramanian M A, Chien C L, Cieplak M Z, Xiao G, Lee V Y, Statt B W, Stronach C E, Kossler W J and Yu X H 1989 *Phys. Rev. Lett.* **62** 2317
[23] Hou X H, Li J Q, Li J W, Xiang J W, Wu F, Huang Y Z and Zhao Z X 1994 *Phys. Rev. B* **50** 496

[24] Roesera H P, Hetfleischa F, Huberb F M, Von Schoenermarka M F, Steppera M, Moritza A and Nikoghosyanc A S 2008 *Acta Astronaut.* **63** 1372

[25] Orlando M T D, Rouver A N, Rocha J R and Cavichini A S 2018 *Phys. Lett. A* **382** 1486

[26] Maeda A, Hase M, Tsukada I, Noda K, Takebayashi S and Uchinokura K 1990 *Phys. Rev. B* **41** 6418

[27] Wei R H, Zhang L, Hu L, Tang X W, Yang J, Dai J M, Song W H, Zhu X B and Sun Y P 2018 *Appl. Phys. Lett.* **112** 251109

[28] Forrò L, Lukatela J and Keszei B 1990 *Solid State Commun.* **73** 501

[29] Chen X H, Yu M, Ruan K Q, Li S Y, Gui Z, Zhang G C and Cao L Z 1998 *Phys. Rev. B* **58** 14219

[30] Maljuk A and Lin C T 2016 *Crystals* **6** 62

[31] Vedeneev S I and Maude D K 2004 *Phys. Rev. B* **70** 184524

[32] Ono S and Ando Y 2003 *Phys. Rev. B* **67** 104512

[33] Sales B C and Chakoumakos B C 1991 *Phys. Rev. B* **43** 12994

[34] Hu L, Zhao M L, Liang S, Song D P, Wei R H, Tang X W, Song W H, Dai J M, He G, Zhang C J, Zhu X B and Sun Y P 2019 *Phys. Rev. Appl.* **12** 044035

[35] Zhang K H L, Du Y, Papadogianni A, Bierwagen O, Sallis S, Piper L F J, Bowden M E, Shutthanandan V, Sushko P V and Chambers S A 2015 *Adv. Mater.* **27** 5191

[36] Wei R H, Tang X W, Hui Z Z, Luo X, Dai J M, Yang J, Song W H, Chen L, Zhu X G, Zhu X B and Sun Y P 2015 *Appl. Phys. Lett.* **106** 101906